Title

Enhanced Charging Kinetics of Porous Electrodes: Surface Conduction as a Short-Circuit Mechanism

Journal

Physical Review Letters, 113(9)

ISSN

0031-9007

Authors

Mirzadeh, Mohammad
Gibou, Frederic
Squires, Todd M

Publication Date

2014-08-29

DOI

10.1103/physrevlett.113.097701

Peer reviewed

Enhanced Charging Kinetics of Porous Electrodes: Surface Conduction as a Short-Circuit Mechanism

Mohammad Mirzadeh and Frederic Gibou
Department of Mechanical Engineering, University of California, Santa Barbara, California 93106, USA

Todd M. Squires*
Department of Chemical Engineering, University of California, Santa Barbara, California 93106, USA

(Received 13 April 2014; published 25 August 2014)

We use direct numerical simulations of the Poisson-Nernst-Planck equations to study the charging kinetics of porous electrodes and to evaluate the predictive capabilities of effective circuit models, both linear and nonlinear. The classic transmission line theory of de Levie holds for general electrode morphologies, but only at low applied potentials. Charging dynamics are slowed appreciably at high potentials, yet not as significantly as predicted by the nonlinear transmission line model of Biesheuvel and Bazant. We identify surface conduction as a mechanism which can effectively "short circuit" the high-resistance electrolyte in the bulk of the pores, thus accelerating the charging dynamics and boosting power densities. Notably, the boost in power density holds only for electrode morphologies with continuous conducting surfaces in the charging direction.

DOI: 10.1103/PhysRevLett.113.097701 PACS numbers: 84.32.Tt, 47.57.jd, 82.45.Gj, 82.47.Uv

Porous electrodes play a central role in various electrochemical devices and technologies, including electrocatalysts [1], batteries [2], fuel cells [3], supercapacitors [4–6], as well as in emerging technologies like capacitive deionization (CDI) [7–10], and "blue" energy harvesting through capacitive mixing of fresh and salt water (CAPMIX) [11–13]. The large surface area per unit volume (or mass) inherent to porous electrodes relative to planar electrodes enhances the rates and magnitude of currents and capacitance that can be achieved. This large surface area, however, is only effective if electrolyte transport occurs quickly enough that all pores are accessible in the relevant time.

The classic "Transmission-Line" (TL) model of de Levie [14], described below, continues to see widespread use in predicting ion transport in porous electrodes. The TL model, however, is built upon linearized electrolyte theories that omit crucial physics at the ~100 mV–1 V potentials relevant for most technologies. A more advanced model, developed by Biesheuvel and Bazant (BB) [15], reveals ion transport to be slowed significantly at the higher potentials relevant for porous electrode processes, reducing the achievable power densities.

Testing the validity of either of these two models, however, would require the full numerical solution of the nonlinear, coupled Poisson-Nernst-Planck (PNP) equations, generally in complex, three-dimensional geometries. Very few direct numerical simulations (DNS) have been performed to study the charging kinetics of porous electrodes, with exceptions limited to low potentials or simple geometries.

Here, we use powerful computational algorithms that we have developed to enable DNS studies of the nonlinear PNP equations, fully resolving transient electric double layers under strong potentials in complex geometries. We directly test both linear (TL) and nonlinear (BB) transmission-line models against the full ion transport dynamics. Curiously, our studies reveal systems whose charging times are *underpredicted* by TL, yet *overpredicted* by BB, even by orders of magnitude. Our DNS results reveal surface conduction (SC), not included in either model, to play the key role in accelerating the charging. We derive a new effective transmission-line model (SC) that incorporates surface conduction and captures the DNS results quantitatively. Significantly, the SC mechanism depends strongly on electrode morphology, unlike previous effective theories, giving an important new quantity to target in the design of high-performance electrochemical systems.

We consider a model supercapacitor [Fig. 1(a)], which stores energy within the electric double layers (EDLs) that form around charged electrodes. The characteristic EDL thickness within symmetric, monovalent, binary electrolytes is given by $\lambda_D = \sqrt{\varepsilon k_B T/2n_\infty e^2}$ [16], wherein n_∞ and e are the ions' number density and elementary charge, ε is the electrolyte permittivity, and $k_B T$ is the thermal energy. At applied potentials lower than the thermal potential

$$\phi_{th} = k_B T/e, \tag{1}$$

EDLs act like linear, parallel plate capacitors, with specific capacitance (per unit area) $c_{EDL} = \varepsilon/\lambda_D$ [16]. Unlike parallel plate capacitors, however, EDLs form conformally over nonplanar electrodes. Therefore, combining the high surface area of porous electrodes (~1000 m^2/g [5]) with the high capacitance per unit area (~10 $\mu F/cm^2$ [4]) of the EDL, yields ultrahigh capacitance per mass. Furthermore, the absence of chemical reactions gives faster charge or discharge

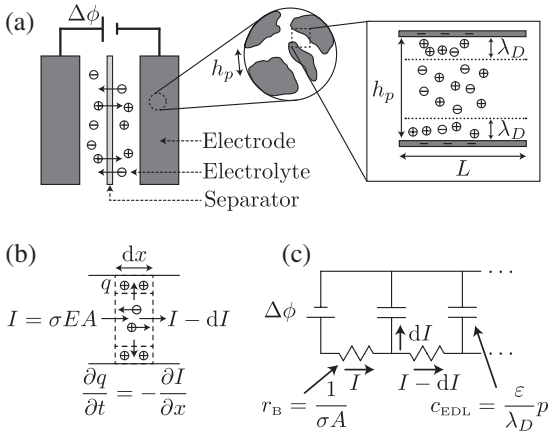

FIG. 1. (a) Macroscopic porous electrodes derive high surface area from the many small pores they contain. The TL model assumes EDL thickness λ_D to be thin compared to the pore size h_p. (b) The charging current drives ions along the pore, some of which are diverted to unscreened electrode sections to form EDLs. Ion conservation gives the TL equation, Eq. (3). (c) The equivalent TL circuit uses linear resistors and capacitors to represent the bulk electrolyte and EDL, respectively.

rates when compared to batteries, for high power density energy storage [4]. Decreasing pore size increases the surface area—and, thus, specific capacitance—of the electrodes, but at the expense of increased ion transport resistance (and, thus, lower power density).

To model the charging dynamics of porous electrodes, we first consider a single pore of perimeter p_p, cross sectional area A_p, and axis $\hat{\mathbf{x}}$ whose walls have been raised to a potential ϕ_e relative to the bulk electrolyte [Fig. 1(b)]. Counterions are driven into the pore (and co-ions out) to form EDLs when they encounter unscreened electrode surfaces. We assume the effective (hydraulic) radius of the pore,

$$h_p = A_p/p_p, \tag{2}$$

to be large relative to the EDL ($h_p \gg \lambda_D$), so that most of the pore is electroneutral. The TL model treats electrode charging in the long-wavelength limit, where variations in electric field $\mathbf{E}$ occur over length scales much longer than h_p, so that $\mathbf{E} \approx -\phi_x(x)\hat{\mathbf{x}}$. This field drives a current $\mathbf{I} = -\sigma\phi_x(x)A_p\hat{\mathbf{x}}$ along the pore, where $\sigma = 2n_\infty e^2 D/k_B T$ with ion diffusivity D. Locally charging the EDL consumes some of this current, and conservation requires $\partial q/\partial t = -\partial I/\partial x$. Assuming constant conductivity σ and linear EDL capacitance $q(x) = c_{EDL}p_p(\phi(x) - \phi_e)$ gives the TL equation,

$$\frac{\partial\phi}{\partial t} = \left(\frac{h_p}{\lambda_D}\right) D\frac{\partial^2\phi}{\partial x^2}. \tag{3}$$

The EDL charging front thus propagates diffusively along the pore, with a charging time scale

$$\tau_{TL} = \frac{\lambda_D}{h_p}\frac{L^2}{D}, \tag{4}$$

for a pore of length L.

While the TL model has been used to interpret experiments [17] and optimize electrode morphologies [18], its assumptions of low potentials and thin EDLs ($\Delta\phi \ll \phi_{th}$ and $\lambda_D/h_p \ll 1$) are often violated in practice [5]. Newman and Tiedemann [2] extended the TL model to include morphological effects via volume-averaging methods and an effective pore radius h_p. The BB model [15] predicts high-potential charging kinetics to be slowed dramatically due to (i) nonlinear EDL capacitance $c_{EDL}(\Delta\phi)$ [19] and (ii) salt depletion in the pores, which decreases the local electrolyte conductivity.

Both TL and BB models approximate the Poisson-Nernst-Planck (PNP) equations for dilute ion transport,

$$\frac{\partial n_\pm}{\partial t} = D\nabla^2 n_\pm \pm \mu e\nabla\cdot(n_\pm\nabla\phi), \tag{5}$$

$$-\nabla^2\phi = \frac{e(n_+ - n_-)}{\varepsilon}, \tag{6}$$

where $\mu = D/k_B T$ is ion mobility and $n_\pm$ are the ion number densities [16]. Direct tests of the TL and BB models require numerical solutions of the full PNP equations, which becomes challenging at high potentials due to the extremely sharp gradients within thin EDLs. The TL model has been validated with the linearized PNP equations for straight pores [20], whereas nonlinear PNP studies of charging kinetics [21] were limited to low electrode potentials.

We have developed a powerful computational algorithm [22] to solve the fully nonlinear PNP equations, by employing Quadtree adaptive grids [23] to resolve strong gradients at reasonable computational cost. Using DNS, we study the effects of applied potential and pore morphology on the charging dynamics of porous electrodes, focusing on thin EDLs in order to directly test the TL and BB models. As a comparison metric, we define the *charging fraction*,

$$\eta(t) = \frac{1}{q_\infty}\int_{\text{pore}} [n_+(t,\mathbf{x}) - n_-(t,\mathbf{x})]dA, \tag{7}$$

which expresses the charge $q(t)$ driven into the electrode as a fraction of the steady-state charge q_∞ that develops at a given potential [24]. The (linearized) TL can be solved exactly to yield $\eta(t) = 1 - \sum_{n=0}^{\infty} 2\lambda_n^{-2}\exp(-\lambda_n^2 t/\tau_{TL})$, where $\lambda_n = n\pi + \pi/2$.

Figure 2(b) shows the charging dynamics $\eta(t)$ computed for three pore morphologies [Fig. 2(a)] at low applied potentials ($\Delta\phi = 0.1\phi_{th}$). When scaled by the naive ion diffusion time L^2/D, these appear to depend on electrode morphology. Properly scaling time by τ_{TL} [Eq. (4)], however, collapses all computations onto the TL prediction, illustrating the TL's quantitative validity for general morphologies at low potentials.

We now examine higher applied potentials, where the TL is expected to fail. Figure 3(a) reveals charging dynamics for a straight-walled pore at $\Delta\phi = 3$, 5, and 7.5 ϕ_{th} to be up to an order of magnitude slower than TL predictions. Such

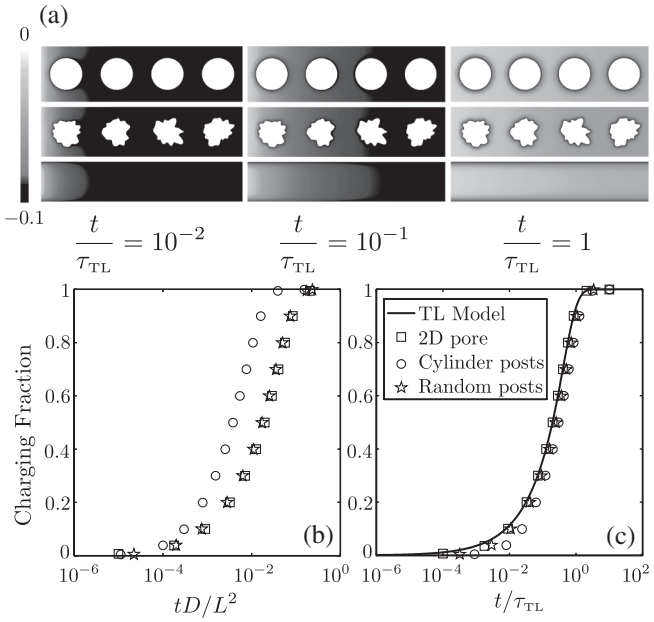

FIG. 2. The computed charging fraction [Eq. (7)] of three model electrodes at $\Delta\phi = 0.1\phi_{th}$. (a) The potential front at three different times looks remarkably similar for three different electrode morphologies. (b) Naively scaling time yields an apparent dependence on electrode morphology. (c) Scaling time by the TL time scale [Eq. (4)] collapses all results onto the TL curve, confirming its validity at low potentials.

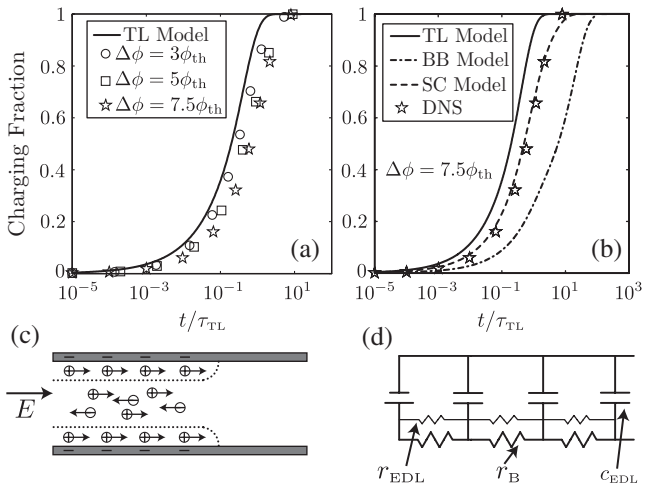

FIG. 3. (a) The charging dynamics computed via DNS for a single straight pore at high potentials are slowed dramatically relative to the TL predictions. (b) Charging time at $\Delta\phi = 7.5\phi_{th}$ is underpredicted by TL, but *overpredicted* by BB. The SC model [Eqs. (12)–(13)], which accounts for excess surface conduction within the EDL, quantitatively captures the charging dynamics. (c) The high conductivity of EDLs at high potentials gives rise to an excess (surface) current. (d) Surface conduction adds a nonlinear resistor r_{EDL} in parallel to that of the bulk pore r_B, which effectively short circuits the high-resistance bulk pores at high potentials to lower the charging time.

slowing is predicted by the BB model, which accounts for both nonlinear EDL capacitance and salt depletion of the pore. Curiously, however, the BB model dramatically *overpredicts* the slowing [Fig. 3(b)].

Detailed DNS results for the charging current (Fig. 4) reveal a strong current within the highly charged EDLs. Such excess surface currents, for example, are known to cause nonmonotonic mobilities in electrophoresis [25]. This surface conduction [16] provides an additional charging pathway [Fig. 3(c)] that enters the effective circuit diagram as a nonlinear resistor in parallel with the bulk resistor [Fig. 3(d)]. Notably, the resistance associated with the surface current is *reduced* as $\Delta\phi$ is increased [16], and ultimately "short circuits" the low-conductance bulk pores to decrease the charging time.

The BB model can be extended to include surface conduction for simple, straight-wall pores as in Fig. 3. The BB model assumes an electroneutral, volume-averaged bulk, and enforces conservation of charge and salt [15]:

$$\frac{\partial}{\partial x}\left(n\frac{\partial\phi}{\partial x}\right) = \epsilon i, \tag{8}$$

$$\frac{\partial n}{\partial t} = \frac{\partial^2 n}{\partial x^2} - \epsilon j, \tag{9}$$

where $n(t,x)$ and $\phi(t,x)$ are area-averaged salt density and electric potential, i and j are the current and salt fluxes into the EDL, and $\epsilon = \lambda_D/h_p$. We now extend the BB model by including the surface currents in the conservation equations for the EDL,

$$\frac{\partial q}{\partial t} = \frac{\partial^2 q}{\partial x^2} + \frac{\partial}{\partial x}\left(w\frac{\partial\phi}{\partial x}\right) + i, \tag{10}$$

$$\frac{\partial w}{\partial t} = \frac{\partial^2 w}{\partial x^2} + \frac{\partial}{\partial x}\left(q\frac{\partial\phi}{\partial x}\right) + j, \tag{11}$$

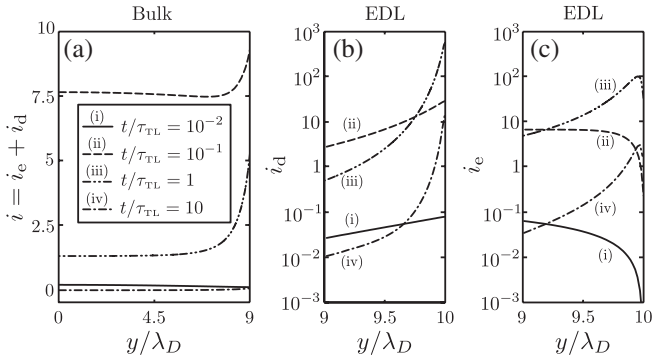

FIG. 4. Axial current densities computed for $\Delta\phi = 7.5\phi_{th}$ in the middle of a single straight pore. (a) The total current in the bulk ($0 < y/\lambda_D < 9$) rises and falls as the charging front passes. Within the EDL ($9 < y/\lambda_D < 10$), the (b) diffusive and (c) Ohmic current densities also rise and fall, but are 2–3 orders of magnitude stronger, revealing the importance of surface conduction at high potentials.

where $q = q(n,\phi) = 2\sqrt{n}\sinh[(\phi-\phi_e)/2]$ and $w = w(n,\phi) = 4\sqrt{n}\sinh^2[(\phi-\phi_e)/4]$ are the excess charge and salt densities in the EDL [15,26]. Eliminating i and j in Eqs. (8)–(11) gives the governing equations for the SC model:

$$\epsilon\frac{\partial q}{\partial t} = \frac{\partial}{\partial x}\left[(n+\epsilon w)\frac{\partial \phi}{\partial x}\right] + \epsilon\frac{\partial^2 q}{\partial x^2}, \tag{12}$$

$$\frac{\partial(n+\epsilon w)}{\partial t} = \frac{\partial^2(n+\epsilon w)}{\partial x^2} + \epsilon\frac{\partial}{\partial x}\left(q\frac{\partial \phi}{\partial x}\right). \tag{13}$$

The total conductivity $(n+\epsilon w)$ includes contributions from the bulk (n) and the excess surface conductivity (ϵw), which becomes large at high potentials. The SC model quantitatively predicts the full DNS results [Fig. 3(b)], and reveals that surface currents enhance the power density of porous electrodes.

To effectively enhance charging kinetics, however, surface conduction requires continuous conducting pathways in the charging direction to short circuit the high-resistance bulk. Whether such paths exist depends on the electrode morphology: surface conduction is much less effective in accelerating the charging of electrodes whose surfaces have discontinuities in the charging direction. Figure 5 shows computed charging dynamics for a "patchy" electrode, with chargeable segments held at a fixed potential [Fig. 5(a)] separated by uncharged segments. These uncharged segments break up the continuous conducting pathways along the charging direction, and render surface conduction ineffective in short circuiting the high-resistance bulk. In this case, the BB model captures the charging dynamics quantitatively. Straight (continuous) pores are accurately described by the SC model for multiple potentials, whereas patchy electrodes obey the slower BB charging kinetics [Fig. 5(d)].

To summarize, our direct numerical simulation (DNS) of the Poisson-Nernst-Planck (PNP) equations have shown the classic Transmission Line (TL) model [14] to be effective in predicting the charging dynamics of electrodes with various morphologies, but only for low potentials. At higher potentials, charging dynamics are slowed dramatically due to the nonlinear capacitance of the EDL, as well as salt depletion of the pores. The BB model [15], which accounts for these nonlinear effects, *overpredicts* the charging time of electrodes with continuous conducting pathways along the charging direction. We have identified surface conductivity within the EDL as the mechanism responsible for "short circuiting" the high-resistance bulk, and shown that the BB approach, modified to include surface conduction, captures the charging dynamics quantitatively. Surface conduction cannot accelerate the charging dynamics of electrodes whose surface morphologies have breaks in the charging direction (e.g., the patchy electrode of Fig. 5), in which case the BB model captures the dynamics.

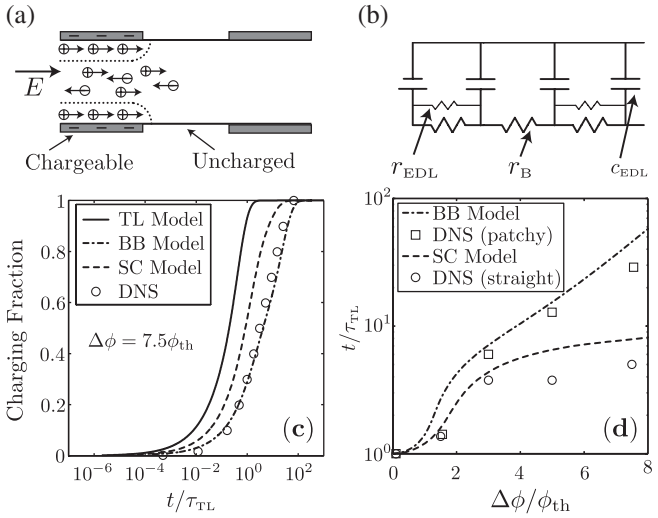

FIG. 5. Charging kinetics of a patchy pore at $\Delta\phi = 7.5\phi_{th}$. (a) A schematic of the patchy pore model in which only selected parts of the electrode surface may charge. (b) The patchy electrode's effective circuit introduces gaps in the low-resistance pathways introduced by surface conductivity, removing the "short circuit" that arose with straight pores [Fig. 3(d)]. (c) The lack of a continuous conducting paths in the charging direction renders surface conduction unable to short circuit the high-resistance bulk. Omitting surface conduction recovers the original BB model, which captures the charging kinetics quantitatively. (d) Charging kinetics are slowed at high applied potentials, accurately described for straight pores by the SC model and for patchy pores by the BB model. The charging time is defined as that required for 99% charging [$\eta(t) = 0.99$].

While electrode morphology has generally been regarded as irrelevant for charging dynamics, our results suggest an unanticipated boost in charging rates for electrodes with appropriate morphologies. One might expect conventional electrodes derived from activated carbon to contain sections that are "dead ends" from a surface conduction standpoint, in which case the slowed (BB) kinetics should hold. Electrodes derived from carbon nanotube forests [27], graphene sheets [28], or hierarchically designed mesoporous carbons [5], on the other hand, naturally introduce the continuous surfaces required for SC "short circuits", and may, thus, boost power densities.

We close by reflecting on the applicability of the PNP equations and the circuit models used in this study. First, the TL, BB, and SC models all assume the EDL to be locally thin compared to the pore radius which is often violated in micropores (radius < 2 nm). Moreover, experiments suggest that EDL capacitance increases in micropores [5], perhaps due to ion-image charge interactions [29]. A modified Donnan (mD) model has recently been developed for micropores, which assumes strongly overlapping EDLs and ion-electrode image charge interactions [30–32], which has successfully described several CDI and CAPMIX experiments [9,12,33–35] in activated carbon electrodes. The results presented here will nonetheless

describe charging dynamics in meso- (radius ~ 5–20 nm) or macropores. The two approaches are complimentary, treating different charging processes within different pore sizes, and it would be interesting to develop a hybrid PNP-mD scheme that blends these two approaches.

Second, the PNP equations are valid for dilute electrolytes in the mean-field limit, assumptions that are almost certainly violated at the high potentials of most applications or for ionic liquid electrolytes [36]. At such high potentials, the PNP equations predict unphysically high ion concentrations in the EDL [37], remedies for which have been proposed via steric repulsions between ions [37–39]. Given that the magnitude of the excess surface current varies with the ion concentration, any reduction in the EDL capacitance (e.g., due to steric repulsions [38] or Stern layers [30,31]) will reduce the effect of surface conductivity. Such reductions affect the SC model as well as the BB model. Irrespective of the quantitative magnitude of the surface conductivity, however, the mechanism we have presented here—wherein excess surface conductivity short circuits the electrode charging dynamics, boosting power densitiy —remains robust, even when steric or other effects reduce the magnitude.

We gratefully acknowledge partial support of the W. M. Keck Foundation, the ONR N00014-11-1-0027, and the Institute for Collaborative Biotechnologies through Grant No. W911NF-09-0001 from the U.S. Army Research Office. The content of the information does not necessarily reflect the position or the policy of the Government, and no official endorsement should be inferred.

*squires@engineering.ucsb.edu

[1] A. J. Bard and L. R. Faulkner, *Electrochemical Methods: Fundamentals and Applications* (John Wiley & Sons, New York, 2000).
[2] J. Newman and W. Tiedemann, AIChE J. **21**, 25 (1975).
[3] R. O'Hayre, S. Cha, W. Colella, and F. B. Prinz, *Fuel Cell Fundamentals* (John Wiley & Sons, Hoboken, NJ, 2005).
[4] R. Kötz and M. Carlen, Electrochim. Acta **45**, 2483 (2000).
[5] P. Simon and Y. Gogotsi, Nat. Mater. **7**, 845 (2008).
[6] B. E. Conway, *Electrochemical Supercapacitors: Scientific Fundamentals and Technological Applications* (Plenum Publishers, New York, 1999).
[7] M. E. Suss, T. F. Baumann, W. L. Bourcier, C. M. Spadaccini, K. A. Rose, J. G. Santiago, and M. Stadermann, Energy Environ. Sci. **5**, 9511 (2012).
[8] S. Porada, R. Zhao, A. van der Wal, V. Presser, and P. M. Biesheuvel, Prog. Mater. Sci. **58**, 1388 (2013).
[9] S. Porada, L. Borchardt, M. Oschatz, M. Bryjak, J. S. Atchison, K. J. Keesman, S. Kaskel, P. M. Biesheuvel, and V. Presser, Energy Environ. Sci. **6**, 3700 (2013).
[10] M. E. Suss, P. M. Biesheuvel, T. F. Baumann, M. Stadermann, and J. G. Santiago, Environ. Sci. Technol. **48**, 2008 (2014).
[11] D. Brogioli, Phys. Rev. Lett. **103**, 058501 (2009).
[12] R. A. Rica, D. Brogioli, and R. Ziano, J. Phys. Chem. C **116**, 16934 (2012).
[13] R. A. Rica, R. Ziano, D. Salerno, F. Mantegazza, and D. Brogioli, Phys. Rev. Lett. **109**, 156103 (2012).
[14] R. de Levie, Electrochim. Acta **8**, 751 (1963).
[15] P. M. Biesheuvel and M. Z. Bazant, Phys. Rev. E **81**, 031502 (2010).
[16] J. Lyklema, *Fundamentals of Interface and Colloid Science. Volume 2: Solid-Liquid Interfaces* (Academic Press, London, 1995).
[17] D. Qu and H. Shi, J. Power Sources **74**, 99 (1998).
[18] M. Eikerling, A. A. Kornyshev, and E. Lust, J. Electrochem. Soc. **152**, E24 (2005).
[19] W. B. Russel, D. A. Saville, and W. R. Schowalter, *Colloidal Dispersions* (Cambridge University Press, Cambridge, 1992).
[20] H. Sakaguchi and R. Baba, Phys. Rev. E **76**, 011501 (2007).
[21] J. Lim, J. D. Whitcomb, J. G. Boyd, and J. Varghese, Comput. Mech. **43**, 461 (2008).
[22] M. Mirzadeh and F. Gibou, J. Comput. Phys. **274**, 633 (2014).
[23] F. Gibou, C. Min, and R. Fedkiw, J. Sci. Comput. **54**, 369 (2013).
[24] M. Mirzadeh, M. Theillard, and F. Gibou, J. Comput. Phys. **230**, 2125 (2011).
[25] R. W. O'Brien and L. R. White, J. Chem. Soc., Faraday Trans. 2 **74**, 1607 (1978).
[26] M. Z. Bazant, K. Thornton, and A. Ajdari, Phys. Rev. E **70**, 021506 (2004).
[27] Z. G. Cambaz, G. Yushin, S. Osswald, V. Mochalin, and Y. Gogotsi, Carbon **46**, 841 (2008).
[28] Y. Zhu, S. Murali, M. D. Stoller, K. J. Ganesh, W. Cai, P. J. Ferreira, A. Pirkle, R. M. Wallace, K. A. Cychosz, M. Thommes, D. Su, E. A. Stach, and R. S. Ruoff, Science **332**, 1537 (2011).
[29] B. Skinner, M. S. Loth, and B. I. Shklovskii, Phys. Rev. Lett. **104**, 128302 (2010).
[30] P. M. Biesheuvel, Y. Fu, and M. Z. Bazant, Phys. Rev. E **83**, 061507 (2011).
[31] P. M. Biesheuvel, Y. Fu, and M. Z. Bazant, Russ. J. Electrochem. **48**, 580 (2012).
[32] P. M. Biesheuvel, S. Porada, M. Levi, and M. Z. Bazant, J. Solid State Electrochem. **18**, 1365 (2014).
[33] R. Zhao, M. van Soestbergen, H. H. M. Rijnaarts, A. van der Wal, M. Z. Bazant, and P. M. Biesheuvel, J. Colloid Interface Sci. **384**, 38 (2012).
[34] S. Porada, L. Weinstein, R. Dash, A. van der Wal, M. Bryjak, Y. Gogotsi, and P. M. Biesheuvel, ACS Appl. Mater. Interfaces **4**, 1194 (2012).
[35] S. Porada, B. B. Sales, H. V. M. Hamelers, and P. M. Biesheuvel, J. Phys. Chem. Lett. **3**, 1613 (2012).
[36] F. Kaasik, T. Tamm, M. M. Hantel, E. Perre, A. Aabloo, E. Lust, M. Z. Bazant, and V. Presser, Electrochem. Comm. **34**, 196 (2013).
[37] M. S. Kilic, M. Z. Bazant, and A. Ajdari, Phys. Rev. E **75**, 021503 (2007).
[38] M. Z. Bazant, M. S. Kilic, B. D. Storey, and A. Ajdari, Adv. Colloid Interface Sci. **152**, 48 (2009).
[39] B. Giera, N. Henson, E. M. Kober, T. M. Squires, and M. S. Shell, Phys. Rev. E **88**, 011301(R) (2013).